HHS Public Access

Author manuscript

Biomaterials. Author manuscript; available in PMC 2016 May 25.

Published in final edited form as:

Biomaterials. 2015 April ; 46: 82–94. doi:10.1016/j.biomaterials.2014.12.046.

Nebulized solvent ablation of aligned PLLA fibers for the study of neurite response to anisotropic-to-isotropic fiber/film transition (AFFT) boundaries in astrocyte–neuron co-cultures

Jonathan M. Zuidema[a,b,1], **Gregory P. Desmond**[a,b,1], **Christopher J. Rivet**[a,b,c], **Kathryn R. Kearns**[a,b], **Deanna M. Thompso**[a,b], and **Ryan J. Gilbert**[a,b,*]

[a]Department of Biomedical Engineering, Rensselaer Polytechnic Institute, Troy, NY 12180, USA

[b]Center for Biotechnology and Interdisciplinary Studies, Rensselaer Polytechnic Institute, Troy, NY 12180, USA

[c]Centro de Investigacion Biomedica, Universidad de los Andes, San Carlos de Apoquindo 2500, Santiago 762001, Chile

Abstract

Developing robust *in vitro* models of *in vivo* environments has the potential to reduce costs and bring new therapies from the bench top to the clinic more efficiently. This study aimed to develop a biomaterial platform capable of modeling isotropic-to-anisotropic cellular transitions observed *in vivo*, specifically focusing on changes in cellular organization following spinal cord injury. In order to accomplish this goal, nebulized solvent patterning of aligned, electrospun poly-L-lactic acid (PLLA) fiber substrates was developed. This method produced a clear topographic transitional boundary between aligned PLLA fibers and an isotropic PLLA film region. Astrocytes were then seeded on these scaffolds, and a shift between oriented and non-oriented astrocytes was created at the anisotropic-to-isotropic fiber/film transition (AFFT) boundary. Orientation of chondroitin sulfate proteoglycans (CSPGs) and fibronectin produced by these astrocytes was analyzed, and it was found that astrocytes growing on the aligned fibers produced aligned arrays of CSPGs and fibronectin, while astrocytes growing on the isotropic film region produced randomly-oriented CSPG and fibronectin arrays. Neurite extension from rat dissociated dorsal root ganglia (DRG) was studied on astrocytes cultured on anisotropic, aligned fibers, isotropic films, or from fibers to films. It was found that neurite extension was oriented and longer on PLLA fibers compared to PLLA films. When dissociated DRG were cultured on the astrocytes near the AFFT boundary, neurites showed directed orientation that was lost upon growth into the isotropic film region. The AFFT boundary also restricted neurite extension, limiting the extension of neurites once they grew from the fibers and into the isotropic film region. This study reveals the importance of anisotropic-to-isotropic transitions restricting neurite outgrowth by itself. Furthermore, we present this scaffold as an alternative culture system to analyze neurite response

*Corresponding author. Rensselaer Polytechnic Institute, Biomedical Engineering, 110 8th Street, Troy, NY 12180-3590, USA. Tel.: +1 518 276 2032. ; Email: gilber2@rpi.edu (R.J. Gilbert)

[1]These authors contributed equally to this work.

Uncited reference: [9].

Appendix A. Supplementary data: Supplementary data related to this article can be found at http://dx.doi.org/10.1016/j.biomaterials.2014.12.046.

to cellular boundaries created following spinal cord injury and suggest its usefulness to study cellular responses to any aligned-to-unorganized cellular boundaries seen *in vivo*.

Keywords

Poly-L-lactic acid; Electrospun fibers; Astrocytes; Fibronectin; Chondroitin sulfate proteoglycan; Dorsal root ganglion

1. Introduction

Greater understanding of the cellular changes in response to biomaterial topography has allowed for biomaterials to be developed that specifically alter cellular behavior to elicit more efficient tissue regeneration [1–3]. Several different modalities of biomaterials are used to examine glial or neuronal responses to micro-and nano-surface topographies. For example, astroglial cells attach more strongly to microfabricated pillars rather than to smooth substrates [4]. Polymer microchannels have been shown to induce hippocampal neuron polarization more so than immobilized nerve growth factor on smooth substrates [5]. Neural cell lines cultured on polymer nanowires induced these neurons to produce more neural markers in comparison to the neural cells cultured on smooth surfaces [6]. Aligned, electrospun fibers, another type of biomaterial topography, directed the extension of neurites [7,8] and helped mature Schwann cell differentiation [8]. Deciphering the mechanisms by which topography influences glial or neuronal behavior in manners supportive of regeneration will lead to better biomaterial technologies to repair the injured nervous system.

Of the topographical biomaterials stated above, aligned, electrospun fibers are most commonly used to mimic the anisotropic structural assembly of axons and glia in the uninjured peripheral nervous system [10] and within the white matter tracts of the uninjured spinal cord [11]. The ability of aligned, electrospun fiber topography to direct regeneration and recreate the anisotropic structure within the peripheral nerve or spinal cord is communicated clearly within recent *in vivo* studies [12–16]. In experimental models of spinal cord injury specifically, electrospun fiber topography was able to encourage a subset of astrocytes to migrate into an electrospun fiber-containing conduit instead of forming an astroglial scar [15]. These studies demonstrate that electrospun fibers have the potential to not only direct axonal regeneration, but also to direct the migration of astrocytes supportive of axonal regeneration.

While it is well established that aligned, electrospun topography has the ability to direct axonal regeneration within experimental models of spinal cord injury, aligned fibers also may be utilized to develop *in vitro* models able to recapitulate transitions from healthy tissue to injured tissue. Studies involving topographical biomaterial constructs present cells with uniform topography, and cellular responses to such topography are compared to separate cultures where cells are cultured on flat surface controls [15,17]. To our knowledge, there are no biomaterial constructs that possess both aligned, electrospun fiber topography and non-topographical features within the same construct. Such constructs would provide information on how cells behave on topographical to non-topographical interfaces within the

same culture, or to create models that mimic injury environments where cells at the lesion interface are not provided with topographical cues.

One injury with an anisotropic-to-isotropic transition is spinal cord injury (SCI), specifically within the white matter tracts. Following SCI, the extracellular environment is drastically altered, leading to changes in the composition and organization of the extracellular matrix. Furthermore, the distribution and alignment of astrocytes at the lesion edge becomes unorganized [11,18]. Immediately following injury, astrocytes migrate to the lesion edge, become hypertrophic and elongated, and create a dense cellular construct (termed the glial scar) [11,18]. These reactive astrocytes at the lesion edge alter the extracellular environment by up-regulating axonal extension-inhibiting chondroitin sulfate proteoglycans (CSPGs) [11,16]. Spared and regenerating axons within the white matter tract then extend to the lesion edge where they become dystrophic [19] and are not likely to cross into the lesion site due to the presence of axonal inhibitors [20,21] and the lack of a bridging scaffold to direct axonal regeneration [22].

Changes in extracellular composition and cellular function are very dynamic following SCI. While *in vivo* rodent models can provide information representative of spinal cord injury within humans [23], the surgeries require exceptional expertise. Additionally, the studies are very time consuming. Therefore, biomaterial constructs possessing topographical and non-topographical domains with a subset of cells found within the spinal cord may be used to assess the efficacy of pharmacological agents or to understand changes in cellular physiology at anisotropic-to-isotropic transitions in a more efficient manner.

In this study, we created anisotropic-to-isotropic fiber/film transition (AFFT) boundaries within electrospun scaffolds depictive of structural changes that occur following white matter SCI using a nebulized solvent technique. Nebulization technologies have been employed in the development of many innovative materials, including the fabrication of nanofiber coatings [24,25], light-emitting electrochemical cell coatings [26], coating and patterning of films with proteins or other molecules [27,28], and cell patterning and implantation [29–31]. The present study expands on previous nebulization technologies by developing a nebulization technique that produces smooth, isotropic topographical regions in aligned PLLA fiber scaffolds. Nebulized chloroform is used to ablate PLLA fibers, creating AFFT boundaries in the PLLA scaffolds. Furthermore, we hypothesized that astrocytes or astrocytes and neurons in co-culture would respond to the scaffold differently depending on whether the cells interfaced with the scaffold in a region with anisotropic topography or with smooth, isotropic topography. Either primary rat astrocytes or co-cultures of astrocytes and dissociated rat DRG neurons were cultured on these scaffolds. Following four days in culture, immunocytochemistry was used to assess astrocyte alignment and ECM orientation differences between anisotropic and isotropic domains. In astrocyte/neuron co-culture experiments, neurite outgrowth in different regions on the scaffold was assessed to examine the ability of growing neurites to extend from anisotropic topographical domains to smooth, isotropic topographical regions.

2. Materials and methods

2.1. Creation of aligned electrospun fibers

To create the aligned, electrospun fibers used here, collection films were first prepared. These films were made via the dissolution of 4 wt.% PLLA (NatureWorks, grade 6201D, Cargill Dow, Minnetonka, MN) in a 50:50 wt.% mixture of chloroform (EMD Millipore, Billerica, MA) and dichloromethane (Macron Chemical, Center Valley, PA). Solution was mixed continuously for 2 h at room temperature until full PLLA dissolution was observed. Afterward, the solution was casted onto 15 × 15 mm, thickness #1 glass cover slips (Knittel Glass, Baunsenweig, Germany) and allowed to dry overnight at 25 °C.

To begin the process of electrospinning, 8 wt.% PLLA was dissolved at room temperature in a 50:50 wt.% mixture of chloroform and dichloromethane. This solution was then electrospun in accordance with procedures previously published by the Gilbert laboratory [8,32]. Fibers were spun using a syringe with a 22 g sharp-tip needle (Fisher Scientific, Hampton, NH), which was insulated to establish high electrical charge only at the needle tip. A variable-speed syringe pump from Razel Scientific (St. Albans, VT) was used to continuously pump the PLLA solution at a rate of 2 ml/h. The working voltage, supplied by a Gamma High Voltage Research power supply (Ormond, FL), was maintained at 10 kV. Fibers were collected onto collection films, which were attached to a spinning aluminum collection wheel (1000 rpm and a diameter of 15 cm) using double sided tape (3M, St. Paul, MN). During electrospinning, the following protocols were employed: distance between the spinning disk and the needle tip was 6 cm, fiber collection time was 20 min, ambient humidity and temperature was controlled between 32–45% and 18–25 °C respectively. For experiments where fibers were to be visualized using epifluorescence microscopy, 10 μg of rhodamine B (Sigma–Aldrich) was added to the electrospinning solution prior to fiber fabrication. Fluorescent fibers were kept isolated from light until cell seeding.

2.2. Creation of AFFT boundary electrospun fiber scaffolds

Smooth, isotropic topological domains were created within the PLLA fiber scaffolds with nebulized chloroform using an airbrushing technique (Fig. S1). First, two 7.5 cm × 2.5 cm glass microscope slides (Electron Microscopy Sciences, Hatfield, PA) were arranged parallel to each other. These slides were then separated by the width of 150 μm. Aligned, PLLA fiber samples were then placed 2 cm beneath the gap separating these slides, with fibers oriented perpendicular to the gap. This 2 cm distance prevented direct contact between fibers and slides, preserving fiber alignment. Chloroform was then airbrushed over the glass slides, selectively dissolving the fibers underneath the gap and creating smooth, isotropic topological domains within the aligned fiber scaffolds. After treatment with nebulized chloroform, fiber scaffolds were sterilized for 12 h at room temperature via ethylene oxide sterilization using 7-L liner bags and 5cc ampoules (Anprolene AN74i, Andersen Products, Haw River, NC).

2.3. Imaging and analysis of AFFT boundary domains and fiber alignment following nebulization

There was concern that nebulization may affect the alignment of fibers near the AFFT boundary. To analyze fiber alignment near the nebulization zone, scanning electron microscopy (SEM) was conducted. SEM micrographs were captured using a Carl Zeiss Supra55 setup with Direct Write Attachment. The fiber samples were attached to glass cover slips using conductive copper tape (3M), scaffold edges were secured to the copper tape using Pelco® Colloidal Silver Liquid (Ted Pella Inc., Redding, CA), and a Denton Desk IV Sputterer (Denton Vacuum, Moorestown, NJ) was used to coat the fiber samples with a 5 nm conductive coating of platinum. Following preparation of fiber scaffolds, SEM micrographs were captured using a 6.6 mm working distance, 20 μm aperture diameter, and a 1.5 kV accelerating voltage. Images were captured using a 3:1 mixing ratio of an in-lens secondary electron detector and a Robinson backscattered electron detector. The resolution of all images was enhanced using line integration scanning ($n = 50$ per line) at a reduced scanning rate.

Fiber diameter, density, and alignment were measured using ImageJ software (National Institutes of Health, Bethesda, MD). Images of five unique scaffolds were used to take these measurements ($n = 5$). To characterize possible effects of nebulized chloroform on fibers, images were taken both near (within 50 μm) and far (greater than 300 μm) from the AFFT boundary. In order to reduce bias, fibers were chosen for measurement using an objective procedure for all measurements. First, a vertical line 200 μm in length was drawn at the geometric center of each image. To measure alignment, the 15 fibers crossing closest to the center of the vertical line were traced. The angle measurements of these fibers were then averaged to find the mean angle of alignment. Differences between this mean and the unique angles of each of the 15 fibers were then found. Differences in alignment were sorted into bins of 2°. To measure fiber diameter, lines were drawn across 20 fibers closest to the center of the vertical reference line. The 20 diameters were then averaged. The density of the PLLA fibers was also measured using ImageJ. To measure density, a 100 μm reference line was drawn perpendicular to the direction of fiber alignment in the center of each image. Fibers completely crossing this reference line were then counted manually.

There was concern following nebulization that there would be a significant height difference between the fibers and the fiber ablation region that may subsequently affect neurite outgrowth from the fibers to the film. Thus, the AFFT boundary was analyzed using atomic force microscopy (AFM). Images of the boundary were captured using an Asylum Research MFP 3D AFM (Asylum Research, Goleta, CA). Two independent scaffolds were imaged using AFM, with three 78 × 78 μm images taken along the AFFT boundary of each. Changes in the height of individual fibers in each image were analyzed as the fibers dissolved into films within the fiber ablation region.

Along with scaffold height change, nebulization could alter the hydrophilicity of the scaffolds which may affect the adhesion of the cells in co-culture. To test this, contact angle goniometry measurements were taken on the scaffold surface. First, half of the aligned fiber scaffold was nebulized with chloroform. This was done in order to create a large nebulized film region, ensuring that water droplets would not touch fibers when testing the surface

character of the nebulized scaffold area. A Ramé-Hart 100 goniometer (Ramé-Hart, Succasunna, NJ) was then used to take contact angle measurements. Measurements were taken on the fibers and nebulized fiber ablated regions of each scaffold. Fiber measurements were taken in both the parallel and perpendicular view. Each measurement was taken using 10 μl of deionized water. Measurements were performed on both uncoated and coated (250 mL of a 2:1 (v/v) mixture of poly-D-lysine (10 mg/ml, Sigma–Aldrich) and fibronectin (10 mg/ml, Sigma–Aldrich) in Hank's Balanced Salt Solution (HBSS, Gibco)) scaffolds in order to determine the effects of coating on hydrophilicity. In either case, three independent scaffolds were used in measurement ($n = 3$).

2.4. Astrocyte isolation and culture

Primary astrocyte cultures from the cerebral cortex of P2 Sprague–Dawley rat pups were isolated as previously described [33] and in accordance with protocols approved by Rensselaer Polytechnic Institute's Institutional Animal Care and Use Committee (IACUC). Briefly, P2 rat pups were euthanized by rapid decapitation. The cerebral cortices were then separated from the meninges, hippocampi, and basal ganglia. The cortical tissue from four animals was minced and transferred to a solution containing TrypLE (Invitrogen, Carlsbad, CA) and OptiMEM (Invitrogen) at a 1:1 dilution. Cells were extracted using three 10-min incubations with TrypLE/OptiMEM additionally supplemented with DNase 1 (Sigma–Aldrich, St. Louis, MO). The second and third extractions were combined with DMEM containing 10% heat inactivated horse serum (HIHS) and 50 U/mL penicillin plus 50 μg/mL streptomycin (P/S, Invitrogen). Cells were pelleted using centrifugation (0.5 RCF for 5 min) and resuspended in an 89/10/1 vol% mixture of Dulbecco's Modified Eagle Medium (DMEM, Gibco, Grand Island, NY), heat inactivated horse serum (HIHS, Invitrogen, Carlsbad, CA), and penicillin/streptomycin (Invitrogen). Dissociated cells were plated at a density of 200,000 cells/flask on poly-D-lysine (Sigma–Aldrich) coated T75 flasks. Flasks were coated for 1 h in a 10 μg/mL solution of poly-D-lysine in Hank's Balanced Salt Solution (HBSS, Gibco) and then washed twice with sterile distilled water prior to astrocyte plating. Astrocytes used in the study were cultured for 2–4 weeks prior to use in experiments. Some cells from each astrocyte isolation were plated onto 15 by 15 mm cover slips coated with poly-D-lysine using methods stated previously to determine astrocyte purity. Only T75 flasks were utilized where the corresponding astrocytes cultured on the glass cover slips contained an astrocyte purity >95%. An astrocyte was confirmed as being an astrocyte using an anti-glial fibrillary acidic protein (GFAP) stain (Dako, Carpinteria, CA). The specific staining procedure used is presented in the Immunocytochemistry section (Section 2.7).

2.5. Culture of astrocytes on AFFT boundary scaffolds

Initially, sterilized PLLA fiber scaffolds were coated with fibronectin (10 μg/mL), since we previously observed astrocytes strongly adhering to fibronectin coated fibers [34]. However, in experiments presented here, we observed astrocyte adhesion to be less at the AFFT interface, so a different coating procedure was devised. In this study, sterilized PLLA scaffolds were coated with 250 μl of a 2:1 (v/v) mixture of poly-D-lysine (10 μg/mL, Sigma–Aldrich) and fibronectin (10 μg/mL, Sigma–Aldrich) in Hank's Balanced Salt Solution (HBSS, Gibco). The mixture was applied and allowed to coat for 1 h at room temperature in a sterile biological hood. The coating solution was then removed, and samples were washed

twice with 250 μl of sterile distilled water. Astrocytes were removed from culture flasks with TrypLE (Invitrogen) and resuspended in astrocyte media. Astrocytes were then seeded onto the PLLA scaffolds at a density of 300,000 cells/cm^2 and cultured in an incubator for 24 h in 250 μl of astrocyte media. After 24 h, 750 μl of astrocyte media was added to each culture, and astrocytes were incubated for an additional 72 h. Astrocytes were concentrated around the AFFT boundaries via the use of polydimethylsiloxane (Dow Corning, Midland, MI) molds. For more in-depth details regarding electrospinning and astrocyte culture methods, see Zuidema et al. [35].

2.6. Neuron isolation and co-culture with astrocytes

Neurons were isolated from the dorsal root ganglia (DRG) of P2 Sprague–Dawley rat pups according to previously established protocols [36] and in accordance to protocols approved by Rensselaer Polytechnic Institute's Institutional Animal Care and Use Committee (IACUC). Briefly, DRG were digested for 50 min in a solution of 0.1 trypsin (MediaTech Inc., Manassas, VA) and 1 mg/mL collagenase A (Sigma–Aldrich) in HBSS. The DRG were then further digested for 10 min in a solution of 0.1% trypsin in HBSS and centrifuged at 100 g. Following centrifugation, DRG were titrated mechanically fifteen times via pipette. Dissociated neurons were preserved at a density of 10^6 cells/mL at a temperature of −80 °C until use.

After allowing the astrocytes to attach to the electrospun fiber scaffolds, PLLA films, or the AFFT scaffolds for 96 h using methods stated in Section 2.5, neurons were plated on top of the adhered astrocytes. Dissociated rat neurons were first centrifuged for 2 min at 2000 rpm. During centrifugation time, astrocyte media was removed from the astrocyte/electrospun fiber scaffolds. After being centrifuged, neurons were mixed with neural growth media. Neural growth media was made in 50 mL increments via a 97/2/1 volume percent mixture of neurobasal media (Invitrogen), B-27 supplement (Life Technologies, Carlsbad, CA), and penicillin/streptomycin (Gibco). To this mixture, 3.7 mL of L-glutamine (Gibco) was added. Neurons were seeded onto astrocytes at a density of 80,000 cells per sample with 150 μl of neural growth media. Care was taken to seed all neurons within 3 mm of the edge of the AFFT boundary via the use of polydimethylsiloxane molds. After 2 h, 850 μl of neural growth media was added to each sample. Astrocyte/neuron co-cultures were then maintained for 24 h before analysis.

2.7. Immunocytochemistry

To visualize astrocytes and neurons following experimentation, the following immunocytochemistry approaches were used. After culture, samples were fixed with a 4% w/v mixture of paraformaldehyde (Sigma–Aldrich) in phosphate buffered saline (PBS) (Invitrogen) for 1 h. Samples were then washed three times with PBS and blocked with a solution consisting of 5% bovine serum albumin (BSA, Sigma–Aldrich) and 0.4% Triton-X (Sigma–Aldrich) in PBS. After removal of the blocking solution, the samples were treated overnight at 4 °C with a dilution of primary antibody stain in incubating solution. Incubating solution consisted of 0.5% BSA and 0.1% Tween-20 (Sigma–Aldrich) in PBS. Primary antibodies used included: rabbit anti-glial fibrillary acidic protein (DAKO Z033429-2; 1:700 dilution), mouse anti-CS56 (Sigma–Aldrich C8035; 1:500), chicken anti-fibronectin

(Sigma–Aldrich GW20021F; 1:500), and chicken anti-neurofilament M (Millipore AB5735, 1:1000). After incubating overnight, the samples were washed three times with a 0.1% solution of Tween-20 in PBS. A secondary stain was then applied in a 1:1000 dilution in incubating solution. Secondary stains used included: donkey anti-mouse (Invitrogen Alexa Fluor 488), goat anti-rabbit (Invitrogen Alexa Fluor 660), and goat anti-chicken (Invitrogen Alex Fluor 488). After 1 h on a shake plate set to 120 rpm at room temperature, samples were treated with a DAPI nuclear stain (Sigma–Aldrich) which was applied to the samples at a concentration of 1 μg/mL in PBS. Fifteen minutes after the application of the DAPI stain, the samples were washed twice with PBS and imaged. All images were obtained using an inverted Olympus IX-81 microscope (Olympus, Tokyo, Japan) and compiled using Adobe Photoshop software (Adobe, San Jose, CA).

2.8. Analysis of astrocyte morphology and the organization of astrocyte extracellular matrix

The morphology of astrocyte structure and extracellular matrix output was analyzed using the Orientation J plug-in [37] for ImageJ. Images from four unique astrocyte cultures were used for analysis ($N = 4$). First, images were adjusted using the Threshold tool to remove background fluorescence. Each image was then divided into a grid system using square bins of 50 × 50 μm. Using Orientation J, the content of each bin was analyzed for directional morphology. In scaffolds with fiber ablated isotropic domains, images acquired were centered upon the isotropic fiber ablation region and included at least 300 μm of aligned fibers on each side of the AFFT boundary. On these images, analysis was first performed using 10 bins located 200 μm to the right of the right-most AFFT boundary. Next, 10 bins located on the right AFFT boundary were analyzed, followed by 10 in the geometric center of the isotropic fiber ablation region. Finally, 10 bins were analyzed at the left boundary and 200 μm to the left of the left boundary, respectively. In images of the samples consisting entirely of fibers or of just films, each image was broken into 50 bins for analysis. Analysis was performed on GFAP to assess astrocyte morphology, and fibronectin (FN) and chondroitin sulfate proteoglycan (CSPG) were analyzed to assess extracellular matrix position and organization.

2.9. Measuring neurite extension in astrocyte–neuron co-cultures

Neurite outgrowth from three unique co-cultures (cultures completed at three different points in time using different cells from separate astrocyte and neuron isolations) ($N = 3$) was traced semi-automatically using Neurolucida software (MBF Bioscience, Wilmington, VT). Individual neurite length was calculated for each neuron after tracing. Additionally, the number of primary neurites (those originating directly from the soma) was calculated for each neuron. Finally, total neurite length and longest neurite were found for each image. Total neurite length was defined as the sum of lengths for each individual neurite, while the longest neurite was defined as the single longest neurite from base to tip.

2.10. Statistical analysis

Images from four cultures were chosen at random for the analysis of the three astrocyte factors (GFAP, FN, or CSPGs). For AFFT boundary scaffold samples, the average orientation of each factor in each portion of the scaffold was compared using one-way

ANOVA testing with statistical significance defined at $p < 0.05$. For analysis of neurite extension, 21 neurons were analyzed from each scaffold type (aligned electrospun fibers, AFFT scaffolds, and a control with smooth topography (PLLA film)). The average total neurite length and longest neurite, were compared using a student's *t*-test with statistical significance defined at $p < 0.05$. All graphs were compiled using mean ± standard error of the mean.

3. Results

3.1. Characterization of AFFT boundary scaffolds

Since other studies show that neurites or neuronal cells respond to differences in fiber diameter [32,38], we wanted to first verify that nebulization would not alter the physical properties of the fibers near the AFFT boundary. Therefore, we started our work by first characterizing the fiber alignment and morphology of PLLA fiber scaffolds using three imaging techniques to reveal the general morphology of fibers and the isotropic film regions. PLLA fibers (Fig. 1A) were imaged using a SEM to produce high magnification images revealing the alignment of fibers. A stereoscope was used to image the AFFT boundaries (Fig. 1B) at lower magnifications to show the overall size of the isotropic film region in the fibers. Fiber diameter, alignment, and density were then compared between control electrospun fiber scaffolds and electrospun fibers that had been subjected to nebulized chloroform. Fiber diameter was similar between the two groups as expected and nebulization did not appear to alter the diameter of the fibers near the AFFT boundary. The average fiber diameter was 3.09 ± 0.25 μm and 3.57 ± 0.21 μm in the non-nebulized samples and in the nebulized samples respectively (Fig. 1C). Fiber alignment was compared between the two groups and both groups were highly aligned with the vast majority of fibers being within 10° from the median fiber angle (Fig. 1D). There were also no significant differences seen between the fiber densities of the two groups; the density was 14.2 ± 0.37 fibers per 100 μm for the control fibers and 13 ± 0.44 fibers per 100 μm for the fibers following creation of the AFFT boundary, respectively (Fig. 1E). These analyses demonstrate that the process of creating AFFT boundaries using nebulized chloroform does not affect the morphology of the fibers except in the isotropic film region. The AFFT isotropic region width was also analyzed, and the average width was found to be 554.85 ± 14.2 μm.

Atomic force microscopy was used to determine how nebulized chloroform affected the scaffold height and scaffold surface (Fig. S2). There was a gradual decrease in height of 0.4 nm/μm at the beginning of the AFFT boundary (Fig. S2A,C). Further into the AFFT boundary, the slope increased to 5 nm/μm (Fig. S2B,D). These results demonstrate a very gradual change in the height of the scaffold. Differences in surface wettability were then analyzed by determining the water contact angles of the scaffolds (Fig. S3). The film region of the AFFT scaffolds was compared to the fibers to see how differences in topography affected the hydrophobicity of the scaffolds. When the scaffolds were not coated with PDL and fibronectin, the film regions were significantly more hydrophilic (85° ± 7.1) than the fibers either parallel to alignment (114.3° ± 2.9) or perpendicular to alignment (117° ± 2.5) (Fig. S3A–C, G). When the AFFT scaffolds were coated with PDL and fibronectin, the hydrophilicity of the fibers parallel to alignment (77° ± 10.4) and perpendicular to alignment

(84.7° ± 6.2) was significantly increased, while no significance was seen between the coated vs. uncoated films (67.3° ± 5.3) (Fig. S3A–G). Importantly, there were no significant differences in surface wettability between the film or fiber regions of the scaffold when they were coated with PDL and fibronectin (Fig. S3D–F, G). Therefore, this factor cannot account for any cellular differences seen between the different regions of the scaffolds.

3.2. Astrocyte morphology on AFFT boundary scaffolds

Once we confirmed that nebulization did not alter fiber physical properties (alignment, diameter, and density), sufficiently alter scaffold depth in nebulized regions, or alter scaffold hydrophobicity, the ability of the scaffolds to promote cellular adhesion and to alter astrocyte morphology was determined. Astrocytes were imaged following four days in culture on fluorescent PLLA fibers (Fig. 2) to examine the ability of the AFFT boundary regions to influence astrocyte morphology. PLLA fibers were fluorescently labeled to show where the fiber ablation region began (Fig. 2A). Astrocytes were then stained against GFAP (Fig. 2B) and imaged to show the changes in their aligned orientation. The overlay of the images demonstrated that the astrocytes are aligned on the fibers while astrocytes in the isotropic fiber ablation region show no preferential alignment (Fig. 2C). The orientation of the astrocytes was then determined at different distances from the AFFT boundary, revealing that astrocytes on the fibers were significantly more aligned than astrocytes located anywhere in the isotropic fiber ablation region (Fig. 2D). Astrocyte morphology was also analyzed at higher magnifications (Fig. S4). Astrocytes growing on aligned fibers have processes that extend in the direction of fiber alignment (Fig. S4 A,B). These processes also appear to take up a greater volume percentage of the cell compared to the astrocytes growing in the fiber ablation region (Fig. S4B,C). The astrocytes growing in the fiber ablation region appear to have larger cell bodies, and their processes extend in all directions without preference (Fig. S4C). These images demonstrate that the AFFT boundary scaffolds can be used to create a transition where cells are oriented on the fibers but have no preferential orientation on the fiber ablation regions of the AFFT boundary scaffolds.

3.3. Astrocytes orient their ECM along the aligned PLLA fibers

Previously, our laboratory has shown that astrocytes cultured on aligned fibers have an aligned cytoskeleton, while the cytoskeletons of astrocytes cultured on PLLA films have no preferential orientation [34]. Similarly, others demonstrated aligned presentation of fibronectin produced by astrocytes cultured on adsorbed laminin patterns [39]. Here, we wanted to examine the ability of aligned, PLLA fibers to orient the presentation of ECM molecules produced by astrocytes and to examine the orientation of ECM within the fiber ablation region of the AFFT scaffolds. CSPGs (Fig. 3) and fibronectin (Fig. 4) were imaged to show their overall orientation on fibers and within the isotropic film region. Fluorescent PLLA fibers (Fig. 3A) and astrocytes (Fig. 3B) were imaged to again demonstrate the changes in astrocyte morphology when on the fibers compared to in the fiber ablation regions. CSPGs were then imaged (Fig. 3C), and the composite image shows the expression of CSPGs compared to astrocyte location on the AFFT boundary scaffolds (Fig. 3D). CSPG expression was somewhat sparse throughout the AFFT boundary scaffolds (Fig. 3C), with limited expression from astrocytes located at any position. High magnification images were used to show the orientation of the disposition of CSPGs at different distances from the

AFFT boundary. These data showed that astrocytes on the fibers presented CSPGs in a significantly more aligned manner (Fig. 3E,G) than astrocytes located anywhere in the fiber ablation region (Fig. 3F,G). Alignment of the fibronectin produced by astrocytes was then determined. Fluorescent PLLA fibers (Fig. 4A) and astrocytes (Fig. 4B) were again imaged to show the presence of astrocytes on the AFFT boundary scaffolds. Astrocyte disposition of fibronectin was imaged (Fig. 4C), and the composite image shows the expression of fibronectin compared to astrocyte location on the AFFT boundary scaffolds (Fig. 4D). Fibronectin was highly expressed by astrocytes at all locations on the AFFT boundary scaffolds (Fig. 4C). High magnification images were used to show the orientation of fibronectin at different distances into and before the AFFT boundary. These data showed that astrocytes on the fibers presented fibronectin in a significantly more aligned manner (Fig. 4E,G) than astrocytes located anywhere in the fiber ablation region (Fig. 4F,G). These results demonstrate that astrocyte alignment affects the alignment of the disposition of astrocyte associated CSPGs and fibronectin.

3.4. Neurite outgrowth on astrocyte seeded AFFT boundary scaffolds

Past studies have demonstrated that neurons cultured on aligned astrocytes extend oriented neurites that grow longer than neurons cultured on astrocytes grown on substrates lacking alignment [39–41]. The AFFT boundary scaffold was designed to expand upon these findings and reveal how neurons interact with astrocytes at an anisotropic-to-isotropic transition. First, neurons were cultured on astrocytes that had been seeded on aligned PLLA fibers (Fig. 5A,D) and PLLA films (Fig. 5B,E) to ensure that astrocytes on PLLA fibers oriented neurite outgrowth compared to astrocytes on PLLA films. Polar histograms were created from the neuron traces, and the histograms demonstrate that neurites on astrocytes and aligned PLLA fibers are oriented in the direction of the fibers (Fig. 5G), while neurites originating from neurons cultured on astrocytes and PLLA films have no preferential alignment (Fig. 5H). Neurons were then cultured on astrocytes cultured on AFFT boundary scaffolds (Fig. 5C,F), and the neurites extending from these neurons were aligned while on the PLLA fibers (Fig. 5I, the right side of the histogram). However, when neurites extended into the fiber ablation region, they began to lose this preferential alignment and their directed growth (Fig. 5I, the left side of the histogram). Total neurite length and the length of the longest neurite were then analyzed for the three groups. Neurites extended significantly longer (1086 ± 329 μm) when cultured on astrocytes and aligned fibers compared to both the film control (500 ± 84 μm) and near the AFFT boundaries (352 ± 65 μm) (Fig. 6A). The length of the average longest neurite of each neuron was then analyzed, and neurons on aligned fibers had an average longest neurite of 224 ± 37 μm and an overall longest neurite of 558 μm. The average longest neurite was significantly longer on fibers compared to the films, whose neurons had an average longest neurite of 125 ± 23 μm and an overall longest neurite of 339 μm, and AFFT boundary scaffolds, whose neurons had an average longest neurite of 145 ± 19 μm and an overall longest neurite of 249 μm (Fig. 6B).

Finally, neurite growth extending into the isotropic film region was analyzed to determine how the AFFT boundary affected neurite outgrowth. Once neurites reached the AFFT boundary, 25% of the neurites stopped and didn't enter the isotropic film region (Fig. 7A,F). The majority of neurites extended less than 100 μm once they reached the AFFT boundary,

with 39% growing between 0 and 50 μm (Fig. 7B,F) and 21% growing between 50 and 100 μm into the isotropic fiber ablation region (Fig. 7C,F). Some neurites did extend greater than 100 μm into the fiber ablation region, with 15% growing over 100 μm once they left the aligned fibers (Fig. 7D–F). These data demonstrate the ability of the AFFT boundaries to affect neurite outgrowth. The anisotropic-to-isotropic transition altered neurite extension to varying degrees, sometimes stopping neurite extension all together or eliminating alignment once the neurites extended from the fibers into the isotropic fiber ablation region.

4. Discussion

This study demonstrates the utility of nebulized solvent ablated electrospun microfiber scaffolds as *in vitro* central nervous system injury models. Nebulized chloroform ablation was able to pattern microfiber scaffolds and not alter the morphological properties of the fibers near the AFFT boundary, while creating a gradual slope from fibers to films. Coating the AFFT scaffolds with PDL and fibronectin produced regions of varying topography that had similar surface wettability profiles. Cultured astrocytes showed distinct morphological differences when growing in the isotropic film region of the AFFT boundary scaffolds compared to on aligned fibers, and the differences in orientation were conveyed to both fibronectin and CSPGs produced by astrocytes. Neurite outgrowth was affected by the transitions from aligned astrocytes on fibers to unorganized astrocytes within the isotropic fiber ablated domains. Neurites extending from the fibers and into the isotropic fiber ablation region were affected by this change in cellular and substrate topography, and their orientation became less aligned while their growth was either stopped or slowed by the substrate transition. Overall, these results validate the use of this new biomaterial model for studying cellular responses to anisotropic-to-isotropic transitions.

The nebulized solvent ablation patterning method used in this study is a robust and straightforward method of creating transitional topographies in polymer based fiber scaffolds. The ease of creating rectangular isotropic film regions in the PLLA fibers (Fig. 1, S1) and the ability to create other shapes based on stencil patterns (Fig. S5) makes this new biomaterial platform an attractive method to further study cellular transitions *in vitro*. While other studies have analyzed cellular responses to changes in fiber alignment [34], fiber diameter [32], and fiber density [42], this study is unique due to the ability of the scaffold to study cellular responses to topological transitions. The formation of isotropic fiber ablation regions in the PLLA fiber scaffolds had no discernable affects on nearby fiber orientation, density, or diameter (Fig. 1). This is important for maintaining consistent fiber physical properties throughout the PLLA fiber scaffold. The gradual slope produced by this method (Fig. S2) limits the effects that changes in height would have on cellular growth. Surface wettability has been shown to affect cellular response to surfaces [43], and the similarities in surface wettability at different regions of the AFFT scaffolds (Fig. S3) suggests that this parameter has no effect on any cellular responses seen in this study.

The AFFT boundary scaffolds presented here allow for the *in vitro* evaluation of cellular responses to isotopic-to-anisotropic topographical transitions. These scaffolds could be valuable for *in vitro* assessment of many injury paradigms (i.e. muscle injuries, tendon injuries, etc.), but our focus was to model the topographic transitions seen in the white

matter tracts after spinal cord injury. Following spinal cord injury, astrocytes at the lesion edge become unorganized and deviate from their typical alignment seen in the healthy spinal cord [11]. Therefore, the astrocytes cultured on aligned fibers represent those aligned tracts, while astrocytes in the isotropic film regions represent the disorganized astrocytes seen in the lesion site. Astrocytes cultured on microfibers clearly aligned in the direction of fiber orientation, but when astrocytes were growing in the isotropic film regions they showed no preferential alignment (Fig. 2). The transition from aligned to non-oriented was abrupt, and astrocytes did not demonstrate preferential alignment even 50 μm into the isotropic film regions (Fig. 2). High magnification images revealed changes in the morphologies of individual astrocytes (Fig. S4). Astrocytes on the fibers projected oriented processes along the fiber direction, while astrocytes growing in the isotropic film regions produced processes that grew non-preferentially (Fig. S4). These results clearly demonstrate the differences between astrocyte growth on the two different areas of the substrate, and the astrocyte alignment also affected the alignment of ECM disposition produced by the astrocytes.

Neurite regeneration following central nervous system (CNS) injury is known to be affected by several ECM molecules produced by astrocytes. CSPGs inhibit neurite outgrowth following nervous system injury, and astrocytes are known to increase their production of CSPGs after CNS injury [11]. Therefore, CSPG orientation was studied to understand how the different topographies affected astrocyte CSPG deposition. CSPGs produced and presented by astrocytes on the fibers were oriented in the direction of astrocyte and fiber alignment, but no alignment was seen from CSPGs presented by astrocytes growing in the isotropic film regions (Fig. 3). The high magnification images clearly depict this phenomenon, and they also demonstrate that CSPGs display a punctate expression pattern when produced by astrocytes growing on either the isotropic film regions or aligned topographies (Fig. 3). Meng et al. have demonstrated similar findings when comparing oriented and non-oriented astrocytes, where their expression of CSPGs is punctate for both morphologies of astrocytes [39]. However, Meng et al. did not see oriented CSPG presentation by aligned astrocytes, which may be due to the differences by which the biomaterials induced astrocyte alignment (Meng et al. used laminin patterning of glass cover slips to impart cellular alignment). This may be due to differences in the size of the laminin patterns (15 μm) relative to the fiber diameter (3 μm), or the curvature effects of the fibers compared to the lack of curvature conveyed by the adsorbed laminin.

Fibronectin is an ECM molecule critical for axon regeneration in the white matter of adult rats [44]. The alignment of fibronectin presented by astrocytes was analyzed, and it was again shown that fibronectin from aligned astrocytes is oriented in the direction of astrocytes and fiber alignment. However, fibronectin shows no preferential alignment when produced by astrocytes growing in the isotropic fiber ablation regions (Fig. 4). There is a substantial amount of fibronectin produced by the astrocytes on both the aligned fibers and within the fiber ablation region, and the high magnification images clearly depict the alignment of this ECM molecule (Fig. 4). These results coincide with those demonstrated by Meng et al. on laminin-patterned substrates, where fibronectin produced by aligned astrocytes adopted the orientation of the astrocytes themselves [39].

While other *in vitro* platforms have focused on studying how neurons are affected by CSPG and laminin gradients [18], chemically activated astrocytes [45], mechanically stretched co-cultures of astrocytes and fibroblasts [46], or mixed glial cell cultures [47], this biomaterial platform was designed to specifically study how neurite extension was affected by astrocyte morphological transitions. Along with other groups, we have previously shown that astrocytes cultured on aligned substrates have altered functions that mostly appear to be supportive of neuron survival and growth when compared to astrocytes cultured on smooth, isotropic substrates [34,39–41,51–53]. In order to evaluate these effects in our AFFT boundary scaffolds, overall neurite extension was first compared between neurons cultured on aligned PLLA fibers, films, or AFFT boundary scaffolds. The orientation of neurite outgrowth was evaluated to determine how the different substrates affected neurite growth. In agreement with several other studies [39–41], we found that neurites extended parallel to astrocytes when cultured on oriented astrocytes (Fig. 5). Neurons cultured on the unorganized astrocytes grown on films demonstrated no preferential neurite extension (Fig. 5). Neurite alignment was then evaluated using the AFFT boundary model. Neurites were evaluated that extended from the aligned fibers and into the isotropic film region. Those that were growing on the fibers maintained highly oriented outgrowth parallel to astrocyte and fiber alignment (Fig. 5). However, once the neurites reached the AFFT boundary and crossed into the isotropic fiber ablation region, they lost their growth guidance and began deviating from their aligned growth (Fig. 5).

The loss in neurite guidance is likely due to the disorganization of the astrocytes within the fiber-free isotropic film region. Previously, Meng et al. provided evidence that neurites follow aligned fibronectin produced by oriented astrocytes [39]. Our data coincides with these results, which provide an explanation for why neurites lose their guidance once they begin growing on the disorganized astrocytes. However, CSPGs are also presented in an aligned manner on the astrocytes cultured on PLLA fibers, and they too lose their alignment when the astrocytes are unaligned. The inhibitory nature of these molecules suggests that when they are aligned, neurites may be guided in a directed manner between several lanes of these molecules. This ability to direct neurite growth through inhibition has been demonstrated previously using an *in vitro* CSPG strip assay [48]. Once the CSPGs are disorganized in the fiber ablation region, the isotropic presentation of CSPGs no longer guides neurites parallel to fiber alignment. These results, taken with the fibronectin results, suggest that the ECM molecules presented by astrocytes have an important effect on the orientation of growth of co-cultured neurons.

Neurons were also evaluated to determine their total neurite length and longest neurites. It was found that neurons cultured on aligned fibers had significantly longer total neurite length and longer average longest neurites compared to the neurons grown on films or near the AFFT boundaries (Fig. 6). The longest neurite on any of the substrates was also observed on the aligned fiber substrate. The fact that there are no differences between extending neurites on films or cultured near the AFFT boundaries led us to more closely investigate what was happening to neurites that extended towards and into the isotropic film regions. Previously, studies by Hynds and Snow [49] and Tom et al. [19] analyzed how neurites grew into cell free regions of adsorbed inhibitory CSPGs *in vitro* by measuring neurite stopping, stalling, turning, or crossing of the inhibitory area. We similarly analyzed

neurites that extended from the fibers into the isotropic fiber ablation region in order to quantify the distance they traveled after encountering this topographical change.

One important aspect of any spinal cord injury model is the ability of the model to restrict neurite outgrowth. Our results demonstrated this capability; it was found that 25% of all the neurites extending towards the gap stopped growing once they reached this boundary, 39% extended between 0 and 50 μm into the isotropic film region, 21% extended 50–100 μm into the isotropic film region, and only 14% extended over 100 μm once they encountered the AFFT boundary (Fig. 7). These data suggest that the transition of astrocytes from oriented to disorganized not only causes neurites to lose directional guidance, but that this boundary also acts to restrict the growth of neurites. The average longest neurite on the AFFT boundary scaffolds was 145 μm, and since only about 7% of the neurites growing in the isotropic film region grew longer than 145 μm, the majority of the longest neurites from each neuron are not neurites that are extending into the isotropic fiber ablation region. Most of the longest neurites for these neurons are extending on the fibers and not encountering the AFFT boundary. Therefore, this growth restriction caused by the boundary between organized and disorganized astrocytes may account for the fact that there are no differences in neurite outgrowth seen between PLLA films and the AFFT boundary scaffolds. This is not as inhibitory as some injury models, such as CSPG gradient models [19,49], where less than 1% of extending neurites grow onto the deposited CSPGs unless a growth supportive ECM molecule (fibronectin or laminin) is present. However, the restriction of neurite outgrowth in this model is due to the change in the orientation of the astrocytes, the molecules that they present, and the substrate topology. Astrocytes produce a variety of factors, and including them in the injury model causes neurons to encounter many different factors while extending neurites.

Recently, a study by Weightman et al. developed an *ex vivo* spinal cord injury model designed to test the viability of biomaterial platforms before they are transplanted *in vivo* [50]. This *ex vivo* model utilizes spinal cord sections that are lesioned with a scalpel and then bridged with poly-lactic acid nanofibers. This model increases the number of biomaterials that can be tested on each animal; however, this *ex vivo* model does not possess the ease of use for an initial analysis that a cell culture model allows. While Weightman et al. developed a robust *ex vivo* model to test biomaterial technologies, this study aimed to develop a biomaterial platform that modeled the injury site.

Our model presents a possible first step in testing therapeutic interventions that increase the growth capacity of neurons. Producing reactive astrocytes in the AFFT boundary system by including a molecular activator in the culture medium could expand on this technology. This should further inhibit neuronal extension in general, and potentially restrict growth even more at the AFFT boundary. Aligned fiber/randomly-oriented fiber boundaries could be fabricated in future studies to gain a better understanding of the importance of an isotropic smooth surface compared to a surface containing micrometer sized fibers that have no preferential alignment. Astrocytes have also been shown to respond to the stiffness of the substrate [54], and previous studies have shown that fibers and films made from the same polymers exhibit different mechanical properties [55,56]. Future studies could include varying the stiffness of the substrates to understand the importance of scaffold mechanical

properties in restricting neurite growth. In any case, our results demonstrate that this anisotropic-to-isotropic fiber/film transition boundary scaffold is a unique *in vitro* model of the organizational transitions of astrocytes encountered by neurons following SCI.

5. Conclusion

The ability to study cellular responses to anisotropic-to-isotropic fiber/film transitions make the AFFT boundary biomaterial scaffolds presented here a unique platform for modeling injury sites *in vitro*. This study demonstrated the ability of the biomaterial to recapitulate the lack of topographical guidance observed following SCI, where extending or regenerating neurites encounter first oriented astrocytes in injury free domains and subsequently unorganized astrocytes at the lesion edge. Astrocytes cultured in the isotropic film regions did not display the alignment observed by astrocytes cultured on oriented PLLA fibers. The differences in astrocyte alignment were also translated in the fibronectin and CSPGs presented by these astrocytes. Neurons cultured onto the astrocytes adopted either oriented neurite outgrowth (on aligned astrocytes) or showed no preferential growth in any axis (unorganized astrocytes). Importantly, the majority of neurites that encountered the AFFT experienced loss of guidance and restricted growth. We suggest that scaffolds similar to those presented here could be useful to validate the ability of pharmacological treatments to spur regeneration in non-topographical domains.

Supplementary Material

Refer to Web version on PubMed Central for supplementary material.

Acknowledgments

We acknowledge the following grant support: NSF CAREER Award 1105125 and NSF I-Corps Grant IIP-1358895 to RJG, and NIH RO1 1RO1EB013281 to DMT. We would like to thank Dr. Linxia Zhang and Christopher Bertucci for their help isolating neurons, and Dr. Sergey Pryshchep for his help with atomic force microscopy.

References

1. Anselme K, Davidson P, Popa AM, Giazzon M, Liley M, Ploux L. The interaction of cells and bacteria with surfaces structured at the nanometer scale. Acta Biomater. 2010; 6:3824–46. [PubMed: 20371386]
2. Hoffman-Kim D, Mitchel JA, Bellamkonda RV. Topography, cell response, and nerve regeneration. Annu Rev Biomed Eng. 2010; 12:203–31. [PubMed: 20438370]
3. Lim JY, Donahue HJ. Cell sensing and response to micro- and nanostructured surfaces produced by chemical and topographic patterning. Tissue Eng. 2007; 13:1879–91. [PubMed: 17583997]
4. Turner AM, Dowell N, Turner SW, Kam L, Isaacson M, Turner JN, et al. Attachment of astroglial cells to microfabricated pillar arrays of different geometries. J Biomed Mater Res. 2000; 51:430–41. [PubMed: 10880086]
5. Gomez N, Lu Y, Chen S, Schmidt CE. Immobilized nerve growth factor and microtopography have distinct effects on polarization versus axon elongation in hippocampal cells in culture. Biomaterials. 2007; 28:271–84. [PubMed: 16919328]
6. Bechara SL, Judson A, Popat KC. Template synthesized poly(epsilon-caprolactone) nanowire surfaces for neural tissue engineering. Biomaterials. 2010; 31:3492–501. [PubMed: 20149440]

7. Corey JM, Lin DY, Mycek KB, Chen Q, Samuel S, Feldman EL, et al. Aligned electrospun nanofibers specify the direction of dorsal root ganglia neurite growth. J Biomed Mater Res A. 2007; 83:636–45. [PubMed: 17508416]
8. Wang HB, Mullins ME, Cregg JM, Hurtado A, Oudega M, Trombley MT, et al. Creation of highly aligned electrospun poly-l-lactic acid fibers for nerve regeneration applications. J Neural Eng. 2009; 6:016001. [PubMed: 19104139]
9. Chew SY, Mi R, Hoke A, Leong KW. The effect of the alignment of electrospun fibrous scaffolds on Schwann cell maturation. Biomaterials. 2008; 29:653–61. [PubMed: 17983651]
10. Bellamkonda RV. Peripheral nerve regeneration: an opinion on channels, scaffolds and anisotropy. Biomaterials. 2006; 27:3515–8. [PubMed: 16533522]
11. Silver J, Miller JH. Regeneration beyond the glial scar. Nat Rev Neurosci. 2004; 5:146–56. [PubMed: 14735117]
12. Chew SY, Mi R, Hoke A, Leong KW. Aligned protein-polymer composite fibers enhance nerve regeneration: a potential tissue-engineering platform. Adv Funct Mater. 2007; 17:1288–96. [PubMed: 18618021]
13. Kim YT, Haftel VK, Kumar S, Bellamkonda RV. The role of aligned polymer fiber-based constructs in the bridging of long peripheral nerve gaps. Biomaterials. 2008; 19:3117–27. [PubMed: 18448163]
14. Gelain F, Panseri S, Antonini S, Cunha C, Donega M, Lowery J, et al. Transplantation of nanostructured composite scaffolds results in the regeneration of chronically injured spinal cords. ACS Nano. 2011; 5:227–36. [PubMed: 21189038]
15. Hurtado A, Cregg JM, Wang HB, Wendell DF, Oudega M, Gilbert RJ, et al. Robust CNS regeneration after complete spinal cord transection using aligned poly-L-lactic acid microfibers. Biomaterials. 2011; 32:6068–79. [PubMed: 21636129]
16. Liu T, Houle JD, Xu J, Chan BP, Chew SY. Nanofibrous collagen nerve conduits for spinal cord repair. Tissue Eng Part A. 2012; 18:1057–66. [PubMed: 22220714]
17. Koppes AN, Zaccor NW, Rivet CJ, Williams LA, Piselli JM, Gilbert RJ, et al. Neurite outgrowth on electrospun PLLA fibers is enhanced by exogenous electrical stimulation. J Neural Eng. 2014; 11:046002. [PubMed: 24891494]
18. Wanner IB, Anderson MA, Song B, Levine J, Fernandez A, Gray-Thompson Z, et al. Glial scar borders are formed by newly proliferated, elongated astrocytes that interact to corral inflammatory and fibrotic cells via STAT3-dependent mechanisms after spinal cord injury. J Neurosci. 2013; 33:12870–86. [PubMed: 23904622]
19. Tom VJ, Steinmetz MP, Miller JH, Doller CM, Silver J. Studies on the development and behavior of the dystrophic growth cone, the hallmark of regenerative failure, in an in vitro model of the glial scar and after spinal cord injury. J Neurosci. 2004; 24:6531–9. [PubMed: 15269264]
20. Sharma K, Slezer ME, Li S. Scar-mediated inhibition and CSPG receptors in the CNS. Exp Neurol. 2012; 237:370–8. [PubMed: 22836147]
21. Pernet V, Schwab ME. The role of Nogo-A in axonal plasticity, regrowth, and repair. Cell Tissue Res. 2012; 349:97–104. [PubMed: 22588543]
22. Cheng H, Cao Y, Olson L. Spinal cord repair in adult paraplegic rats: partial restoration of hind limb function. Science. 1996; 273:510–3. [PubMed: 8662542]
23. Cheriyan T, Ryan DJ, Weinreb JH, Cheriyan J, Paul JC, Lafage V, et al. Spinal cord injury models: a review. Spinal Cord. 2014 in press.
24. Chao Z, Kapetanovic A, Deng Y, Rolandi M. A chitin nanofiber ink for air-brushing, replica molding, and microcontact printing of self-assembled macro-, micro-, and nanostructures. Adv Mater. 2011; 23:4776–81. [PubMed: 21948304]
25. Tutak W, Sarkar S, Lin-Gibson S, Farooque TM, Jyotsnendu G, Wang D, et al. The support of bone marrow stromal cell differentiation by airbrushed nanofiber scaffolds. Biomaterials. 2013; 34:2389–98. [PubMed: 23312903]
26. Sandström A, Asadpoordarvish A, Enevold J, Edman L. Spraying light: ambient-air fabrication of large-area emissive devices on complex-shaped surfaces. Adv Mater. 2014 in press.

27. Guillaume O, Garric X, Lavigne JP, Van Den Berghe H, Coudane J. Multilayer, degradable coating as a carrier for the sustained release of antibiotics: preparation and antimicrobial efficacy in vitro. J Control Release. 2012; 162:492–501. [PubMed: 22902589]
28. Westedt U, Wittmar M, Hellwig M, Hanefeld P, Greiner A, Schaper AK, et al. Paclitaxel releasing films consisting of poly (vinyl alcohol)-graft-poly (lactide-co-glycolide) and their potential as biodegradable stent coatings. J Control Release. 2006; 2006(111):235–46. [PubMed: 16466824]
29. de Windt TS, Vonk LA, Buskermolen JK, Visser J, Karperien M, Bleys RL, et al. Arthroscopic airbrush assisted cell implantation for cartilage repair in the knee: a controlled laboratory and human cadaveric study. Osteoarthr Cartil. 2014 in press.
30. Nahmias Y, Arneja A, Tower TT, Renn MJ, Odde DJ. Cell patterning on biological gels via cell spraying through a mask. Tissue Eng. 2005; 11:701–8. [PubMed: 15998211]
31. Veazey W, Anusavice KJ, Moore K. Mammalian cell delivery via aerosol deposition. J Biomed Mater Res B Appl Biomater. 2005; 72:334–8. [PubMed: 15546150]
32. Wang HB, Mullins ME, Cregg JM, McCarthy CW, Gilbert RJ. Varying the diameter of aligned electrospun fibers alters neurite outgrowth and Schwann cell migration. Acta Biomater. 2010; 6:2970–8. [PubMed: 20167292]
33. Mongin AA, Hyzinski-Garcia MC, Vincent MY, Keller RW Jr. A simple method for measuring intracellular activities of glutamine synthetase and glutaminase in glial cells. Am J Physiol Cell Physiol. 2011; 301:C814–22. [PubMed: 21734190]
34. Zuidema JM, Hyzinski-Garcia MC, Van Vlasselaer K, Zaccor NW, Plopper GE, Mongin AA, et al. Enhanced GLT-1 mediated glutamate uptake and migration of primary astrocytes directed by fibronectin-coated electrospun poly-l-lactic acid fibers. Biomaterials. 2014; 35:1439–49. [PubMed: 24246642]
35. Zuidema, JM.; Hyzinski-García, MC.; Mongin, AA.; Gilbert, RJ. Extracellular Matrix. New York: Springer; 2015. Cultivation and imaging of astrocytes on protein-coated fluorescent topographies constructed from aligned PLLA electrospun fibers; p. 181-195.
36. Koppes AN, Seggio AM, Thompson DM. Neurite outgrowth is significantly increased by the simultaneous presentation of Schwann cells and moderate exogenous electric fields. J Neural Eng. 2011; 8:046023. [PubMed: 21712572]
37. Rezakhaniha R, Agianniotis A, Schrauwen JTC, Griffa A, Sage D, Bouten CVC, et al. Experimental investigation of collagen waviness and orientation in the arterial adventitia using confocal laser scanning microscopy. Biomech Model Mechanobiol. 2012; 11:461–73. [PubMed: 21744269]
38. Christopherson GT, Song H, Mao HQ. The influence of fiber diameter of electrospun substrates on neural stem cell differentiation and proliferation. Biomaterials. 2009; 30:556–64. [PubMed: 18977025]
39. Meng F, Hlady V, Tresco PA. Inducing alignment in astrocyte tissue constructs by surface ligands patterned on biomaterials. Biomaterials. 2012; 33:1323–35. [PubMed: 22100982]
40. Chow WN, Simpson DG, Bigbee JW, Colello RJ. Evaluating neuronal and glial growth on electrospun polarized matrices: bridging the gap in percussive spinal cord injuries. Neuron Glia Biol. 2007; 3:119–26. [PubMed: 18458759]
41. Biran R, Noble MD, Tresco PA. Directed nerve outgrowth is enhanced by engineered glial substrates. Exp Neurol. 2003; 184:141–52. [PubMed: 14637087]
42. Xie J, Liu W, MacEwan MR, Bridgman PC, Xia Y. Neurite outgrowth on electrospun nanofibers with uniaxial alignment: the effects of fiber density, surface coating, and supporting substrate. ACS Nano. 2014; 8:1878–85. [PubMed: 24444076]
43. Dowling DP, Miller IS, Ardhaoui M, Gallagher WM. Effect of surface wettability and topography on the adhesion of osteosarcoma cells on plasma-modified polystyrene. J Biomater Appl. 2011; 26:327–47. [PubMed: 20566655]
44. Tom VJ, Doller CM, Malouf AT, Silver J. Astrocyte-associated fibronectin is critical for axonal regeneration in adult white matter. J Neurosci. 2004; 24:9282–90. [PubMed: 15496664]
45. Yu P, Wang H, Katagiri Y, Geller HM. An in vitro model of reactive astrogliosis and its effect on neuronal growth. Methods Mol Biol. 2012; 814:327–40. [PubMed: 22144316]

46. Wanner IB, Deik A, Torres M, Rosendahl A, Neary JT, Lemmon VP, et al. A new in vitro model of the glial scar inhibits axon growth. Glia. 2008; 56:1691–709. [PubMed: 18618667]
47. Achyuta AKH, Polikov VS, White AJ, Lewis HGP, Murthy SK. Biocompatibility assessment of insulating silicone polymer coatings using an in vitro glial scar assay. Macromol Biosci. 2010; 10:872–80. [PubMed: 20503195]
48. Vahidi B, Park JW, Kim HJ, Jeon NL. Microfluidic-based strip assay for testing the effects of various surface-bound inhibitors in spinal cord injury. J Neurosci Methods. 2008; 170:188–96. [PubMed: 18314199]
49. Hynds DL, Snow DM. Fibronectin and laminin elicit differential behaviors from SH-SY5Y growth cones contacting inhibitory chondroitin sulfate proteoglycans. J Neurosci Res. 2001; 66:630–42. [PubMed: 11746383]
50. Weightman AP, Pickard MR, Yang Y, Chari DM. An in vitro spinal cord injury model to screen neuroregenerative materials. Biomaterials. 2014; 35:3756–65. [PubMed: 24484676]
51. Lau CL, Kovacevic M, Tingleff TS, Forsythe JS, Cate HS, Merlo D, et al. 3D Electrospun scaffolds promote a cytotrophic phenotype of cultured primary astrocytes. J Neurochem. 2014 in press.
52. Puschmann TB, Zand C, De Pablo Y, Kirchhoff F, Pekna M, Liu J, et al. Bioactive 3D cell culture system minimizes cellular stress and maintains the in vivo-like morphological complexity of astroglial cells. Glia. 2013; 61:432–40. [PubMed: 23292921]
53. Mattotti M, Alvarez Z, Ortega JA, Planell JA, Engel E, Alcantara S. Inducing functional radial glia-like progenitors from cortical astrocyte cultures using micropatterned PMMA. Biomaterials. 2012; 33:1759–70. [PubMed: 22136716]
54. Moshayedi P, da F Costa L, Christ A, Lacour SP, Fawcett J, Guck J, et al. Mechanosensitivity of astrocytes on optimized polyacrylamide gels analyzed by quantitative morphometry. J Phys Condens Matter. 2010; 22:194114. [PubMed: 21386440]
55. Kwon IK, Kidoaki S, Matsuda T. Electrospun nano-to microfiber fabrics made of biodegradable copolyesters: structural characteristics, mechanical properties and cell adhesion potential. Biomaterials. 2005; 26:3929–39. [PubMed: 15626440]
56. Kidoaki S, Kwon IK, Matsuda T. Structural features and mechanical properties of in situ-bonded meshes of segmented polyurethane electrospun from mixed solvents. J Biomed Mater Res B Appl Biomater. 2006; 76:219–29. [PubMed: 16044432]

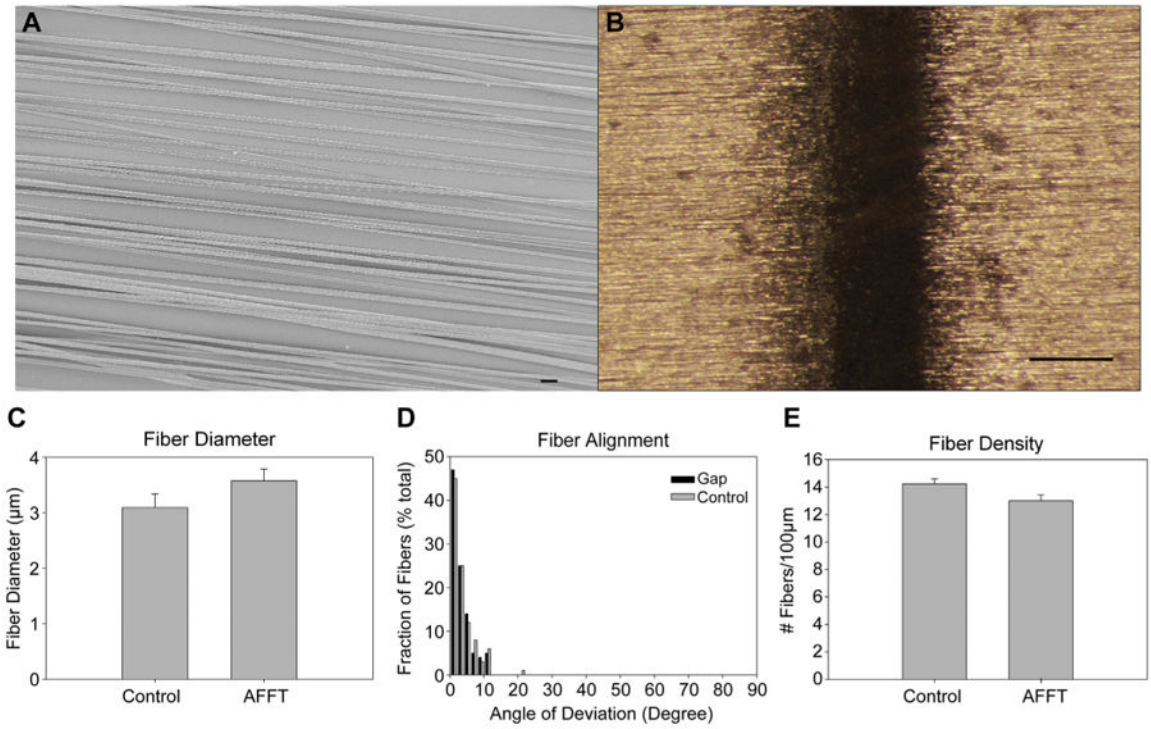

Fig. 1.

Characterization of PLLA fiber/AFFT scaffolds. (A) SEM micrograph of aligned electrospun fibers. (B) Stereoscope image showing fiber ablation region within fiber scaffold. (C–E) Quantitative comparison of fiber diameter (C), fiber alignment (D), and fiber density (E) in control and AFFT scaffolds show no significant differences. Scale bars in (A) and (B) of 10 μm and 500 μm, respectively. Data in (C) and (E) are mean values ± SE from five independently fabricated scaffolds.

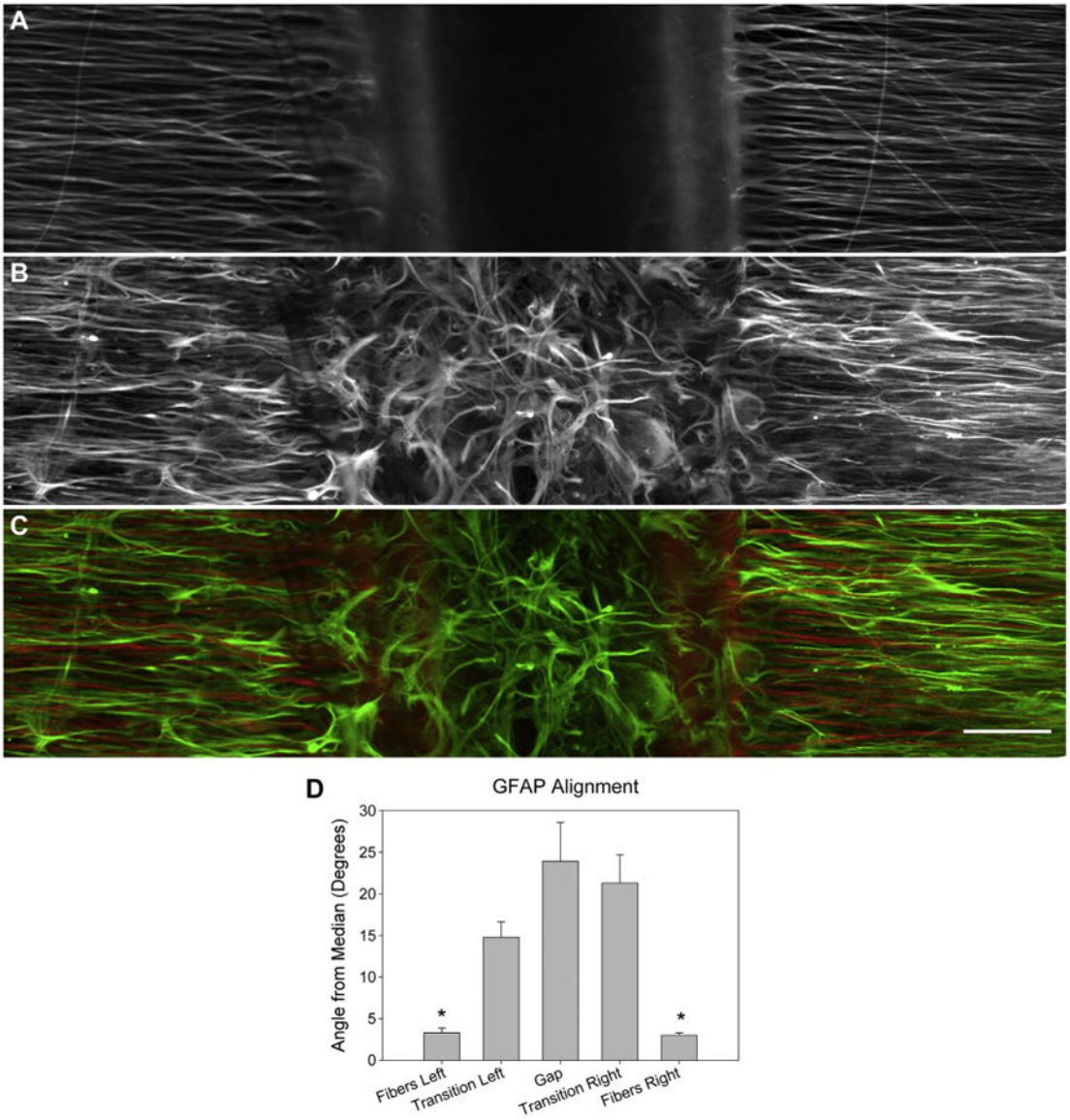

Fig. 2.

Astrocytes cultured on AFFT scaffolds show varying alignment depending on their location on the scaffold. (A–C) 20× magnification images of a fluorescently-labeled fiber/AFFT scaffold (A), astrocytes cultured on the scaffold (B), and a merge of the two (C). (D) Quantification of astrocyte alignment at various locations within the scaffold. Scale bar = 100 μm in C and can be applied to images A and B. Green signal represents GFAP in (C), while red signal is produced by rhodamine B within the fibers. Signal seen within the fiber ablation region appears due to leftover rhodamine following fiber dissolution. Data in (D) represent the mean values ± SE from four independently prepared cultures. * indicates statistical significance. (For interpretation of the references to color in this figure legend, the reader is referred to the web version of this article.)

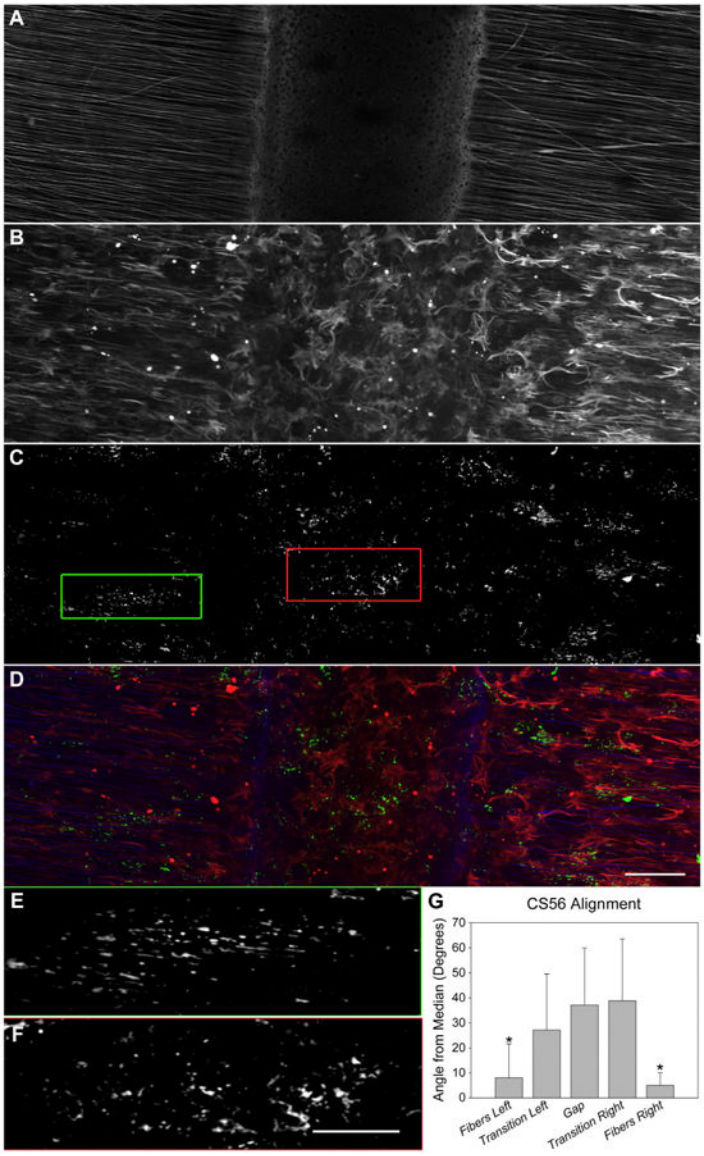

Fig. 3.

Alignment of astrocyte-produced CSPGs is disrupted within the AFFT scaffold. (A–D) 20× magnification images of fluorescently-labeled fiber/AFFT scaffold (A), astrocytes cultured on scaffold (B), CSPGs produced by astrocytes (C), and a merge of the three (D). (E) Magnified image of aligned CSPGs from astrocytes on aligned scaffold region. (F) Magnified image of unaligned CSPGs from astrocytes within the fiber ablation region. (G) Quantification of CSPG alignment at various locations within scaffold. Scale bar in D = 100 μm and can be applied to A, B, and C. Scale bar in F = 50 μm and can be applied to E. Green signal in (D) represents CSPGs, red signal represents GFAP, and blue signal represents rhodamine B within fibers. Data in (G) represent mean values ± SE from four independently prepared cultures. * indicates statistical significance. (For interpretation of the references to color in this figure legend, the reader is referred to the web version of this article.)

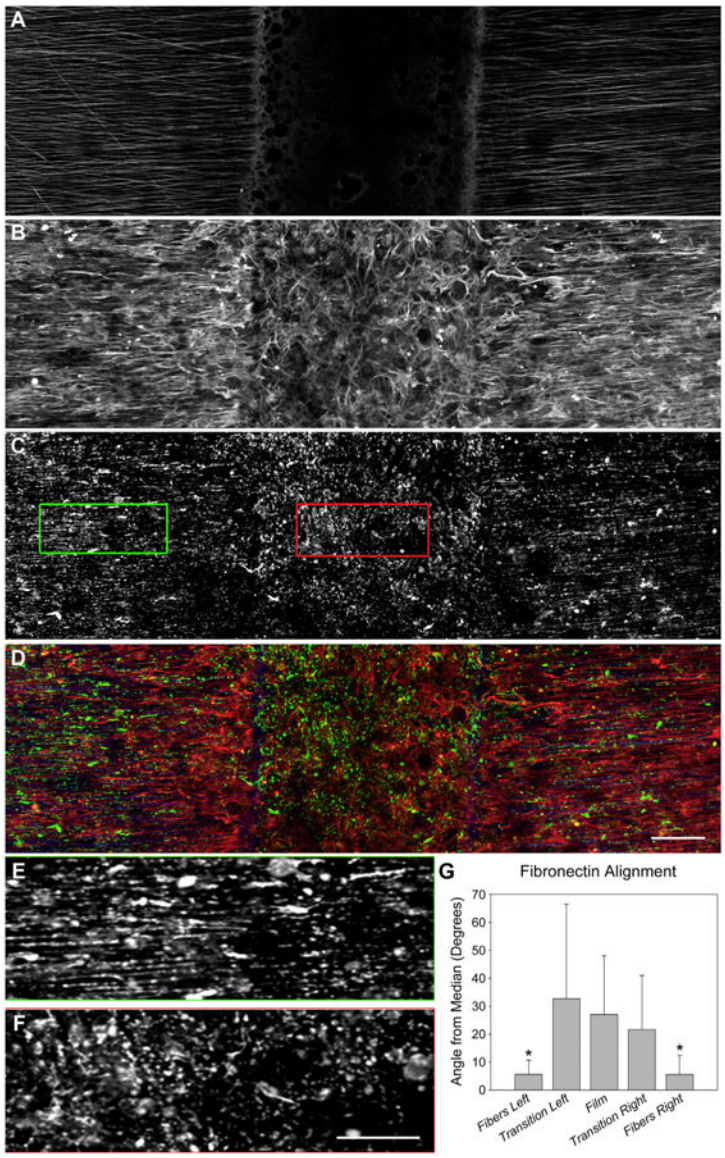

Fig. 4.

Alignment of astrocyte-produced fibronectin is disrupted within the AFFT scaffold. (A–D) 20× magnification images of fluorescently-labeled fiber/AFFT scaffold (A), astrocytes cultured on scaffold (B), fibronectin from astrocytes (C), and a merge of the three (D). (E) Magnified image of aligned fibronectin produced by astrocytes on aligned scaffold region. (F) Magnified image of unaligned fibronectin produced by astrocytes in the fiber ablation region. (G) Quantification of CSPG alignment at various locations within scaffold. Scale bar in D = 100 μm and can be applied to A, B, and C. Scale bar in F = 50 μm and can be applied to E. Green signal in (D) represents fibronectin, red signal represents GFAP, and blue signal represents rhodamine B within fibers. Data in (G) represent mean values ± SE from four independently prepared cultures. * indicates statistical significance. (For interpretation of the references to color in this figure legend, the reader is referred to the web version of this article.)

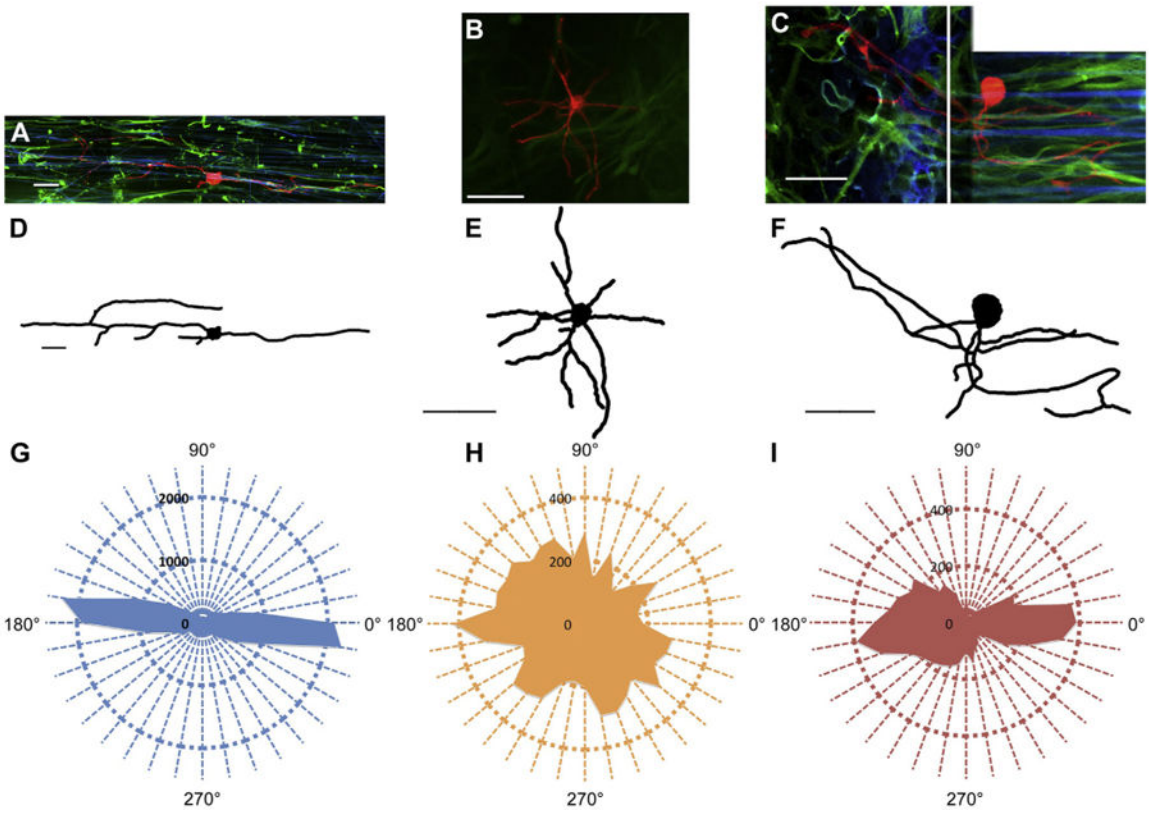

Fig. 5.

Directed neurite growth is disrupted by the anisotropic-to-isotropic transition. (A–C) 40× fluorescent images of individual neurons seeded on astrocytes which were cultured on aligned fiber scaffolds (A), PLLA films (B), or fiber/AFFT scaffolds (C). (D–F) Isolated traces of individual neurons pictured in A, B, and C, respectively. (G–I) Polar histograms showing total outgrowth and orientation of neurites seeded on astrocyte layers which were cultured on the three scaffold types (G = aligned fibers, H = film, I = AFFT boundary). Histogram I shows a transition from aligned neurite growth (right of histogram) to unaligned growth (left) upon neurite growth into the fiber ablation region. Scale bars in A–F = 50 μm. Green signal in fluorescent images represents GFAP, red signal represents neurofilament, and blue signal represents rhodamine B within fibers. White line in G marks the beginning of the fiber-free gap. (For interpretation of the references to color in this figure legend, the reader is referred to the web version of this article.)

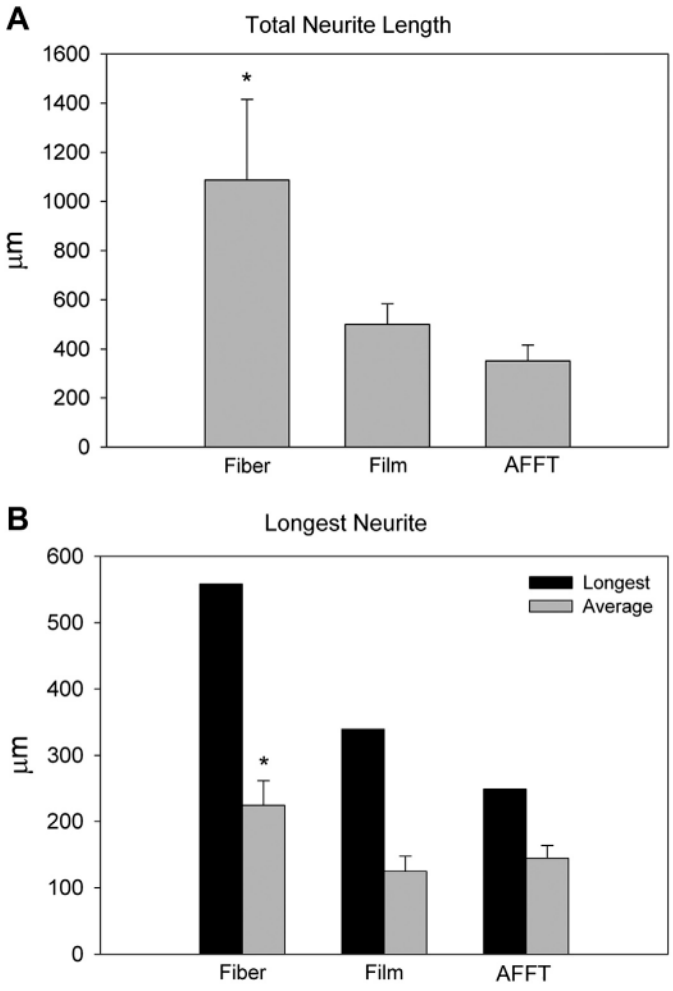

Fig. 6.

Quantitative comparison of neurite outgrowth on aligned fibers, films, and AFFT scaffolds. (A) Comparison of total neurite length shows significantly greater length on aligned fibers than on films or AFFT scaffolds ($p < 0.05$). (B) Comparison of single longest neurite length (black) and average longest neurite length (gray). Average longest neurites are significantly longer on aligned fibers ($p < 0.05$) than other two scaffolds. Data for all plots taken from three independent cultures. * signifies statistical significance.

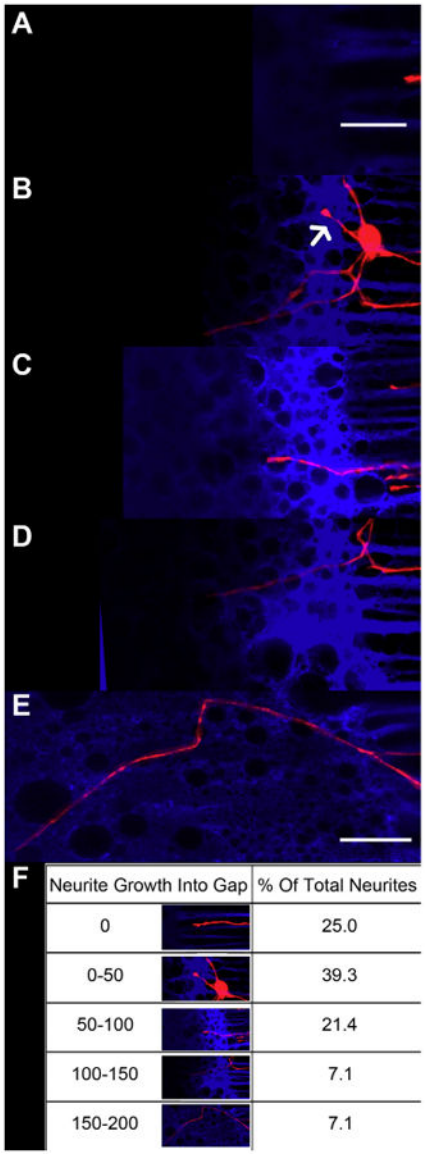

Fig. 7.

Neurite growth is disrupted by the fiber ablation region of the AFFT boundary scaffolds. (A–E) 40× magnification images of neurites which either failed to grow into fiber ablation region (A), or grew: less than 50 μm (B), between 50 and 100 μm (C), between 100 and 150 μm (D), or greater than 150 μm into fiber ablation region (E). No neurite growth greater than 200 μm into the fiber ablation region was seen. (F) Quantification of the proportion of neurites that grew within each distance bin into the fiber ablation region. Scale bar in A = 25 μm, while the scale bar in E = 50 μm and can be applied to B, C, and D. Blue signal in (A–E) represents rhodamine B present in fibers, while red signal represents neurofilament. Rhodamine-derived blue signal is present in fiber ablation region due to the dissolution of fluorescently-labeled fibers. Data in F are derived from analysis of 21 individual neurons, all seeded within 50 μm of AFFT boundary. (For interpretation of the references to color in this figure legend, the reader is referred to the web version of this article.)